Electronic Supplementary Material (ESI) for Molecular BioSystems

Supplementary Data

ATP regulation of the ligand-binding properties in temperate and cold-adapted haemoglobins. X-ray structure and ligand-binding kinetics in the sub-Antarctic fish *Eleginops maclovinus*

Daniela Coppola[a], Stefania Abbruzzetti[b], Francesco Nicoletti[c], Antonello Merlino[de], Alessandra Gambacurta[f], Daniela Giordano[a], Barry D. Howes[c], Giampiero De Sanctis[g], Luigi Vitagliano[e], Stefano Bruno[h], Guido di Prisco[a], Lelio Mazzarella[de], Giulietta Smulevich[c], Massimo Coletta[i], Cristiano Viappiani[b], Alessandro Vergara[de*], Cinzia Verde[a*]

[a]Institute of Protein Biochemistry, CNR, Via Pietro Castellino 111, I-80131 Naples, Italy
[b]Dipartimento di Fisica, Università degli Studi di Parma, viale delle Scienze 7A, 43124 Parma, Italy and Istituto Nanoscienze, CNR, Piazza San Silvestro 12 - 56127 Pisa, Italy
[c]Dipartimento di Chimica "Ugo Schiff", Università di Firenze, Via della Lastruccia 3-13, 50019 Sesto Fiorentino (FI), Italy
[d]Department of Chemical Sciences, University of Naples "Federico II", Complesso Universitario Monte S. Angelo, Via Cinthia, 80126 Naples, Italy
[e]Istituto di Biostrutture e Bioimmagini, CNR, Via Mezzocannone 6, I-80134 Naples, Italy.
[f]Dipartimento di Medicina Sperimentale e Chirurgia, Università di Roma Tor Vergata, Via Montpellier 1, 00133 Roma, Italy
[g]Scuola di Bioscienze e Biotecnologie, Università di Camerino, 62032 Camerino (MC), Italy
[h]Dipartimento di Biochimica e Biologia Molecolare, Università di Parma, Viale G.P. Usberti 23/A, 43100 Parma, Italy
[i]Department of Clinical Sciences and Translational Medicine, Università di Roma Tor Vergata, Via Montpellier 1, 00133 Rome, Italy and Interuniversity Consortium for the Research on the Chemistry of Metals in Biological Systems, Via C. Ulpiani 27, 70126 Bari, Italy

[*]Corresponding authors: Cinzia Verde, Tel/Fax: 0816132710, email: c.verde@ibp.cnr.it and Alessandro Vergara, Tel: 081674259, Fax: 081674070, email: avergara@unina.it.

Crystal structure determination and refinement

Using the dialysis technique, two different crystal forms were obtained in the same crystallisation vial. One crystal form has orthorhombic symmetry (space group $P2_12_12_1$) with unit-cell parameters a=58.18 Å, b=88.08 Å, c=123.20 Å and one tetramer in the asymmetric unit. The second form is hexagonal (space group $P6_122$) with unit-cell parameters a=91.70 Å, b=168.72 Å and one dimer αβ in the asymmetric unit. In the orthorhombic crystals, which show better diffraction quality, data collections were performed using a Rigaku Micromax 007 HF generator equipped with a Saturn944 CCD detector, at 298 and 100 K. The structure was solved by molecular replacement using the program AMoRE[1] and the structure of partially oxidised *Tb*Hb (Protein Data Bank code 2GK3) as search model.[2] The refinement of the structure at the two different temperatures was performed using the program SHELX.[3]

Refinement runs were followed by manual intervention, using the molecular graphics program O[4] mainly to correct side chain conformations. Water molecules were identified by evaluating the shape of the electron density and the distance of potential hydrogen bond donors and/or acceptors. The refinement ended with an R-factor of 0.212 (Rfree 0.253) for data collected at 100 K, and an R-factor of 0.229 (Rfree 0.254) for room temperature data.

Table SI. Diffraction data and refinement statistics of *Em*Hb1-CO crystals.

Space Group	$P2_12_12_1$ (T=100 K)	$P2_12_12_1$ (T= 298 K)
Cell parameters		
a(Å)	58.175	58.473
b(Å)	88.075	89.888
c(Å)	123.194	125.278
Asymmetric unit content	$\alpha_2\beta_2$ tetramer	$\alpha_2\beta_2$ tetramer
Resolution range (Å)	50-1.45 (1.50-1.45)	50-2.05 (2.12-2.05)
No. of total reflections	384398	108997
No. of unique reflections	109738	40284
Completeness (%)	97.3 (90.8)	95.2 (95.2)
Redundancy	3.5 (2.5)	2.7 (2.6)
R_{merge} (%)	0.075 (0.384)	0.095 (0.580)
Wilson B-factor ($Å^2$)	13.5	
I/σ	37.5 (3.3)	7.4 (2.2)
Rfactor/Rfree	0.212/0.253	0.229/0.254
Number of protein atoms	4476	4422
Number of water molecules	408	26
Number of glycerol molecules	1	0
B-factor (all atoms) ($Å^2$)	21.8	45.9
Ramachandran plot statistics		
Residues in the most favored regions (%)	93.7	93.7
Residues in the additionally allowed regions (%)	6.3	6.3
Residues in the generously allowed regions (%)	-	-
Root mean square deviations from ideality		
Bond distances (Å)	0.009	0.005
Bond angles (°)	2.008	1.683
Geometry validation		
Close contacts in the asymmetric unit	none	none
Close contacts based on crystal symmetry	none	none

Table SII. Structural features of the CO binding to haem

	α_1	β_1	α_2	β_2
Fe-N(prox His) distance (Å)	2.12	2.15	2.09	1.94
Fe-C(CO) distance (Å)	1.71	2.02	1.74	2.06
Fe-CO angle (°)	169.0	177.4	162.3	168.9
distance of the Fe from the plane of the pyrrole nitrogen atoms (Å)	0.01	0.03	0.00	0.00

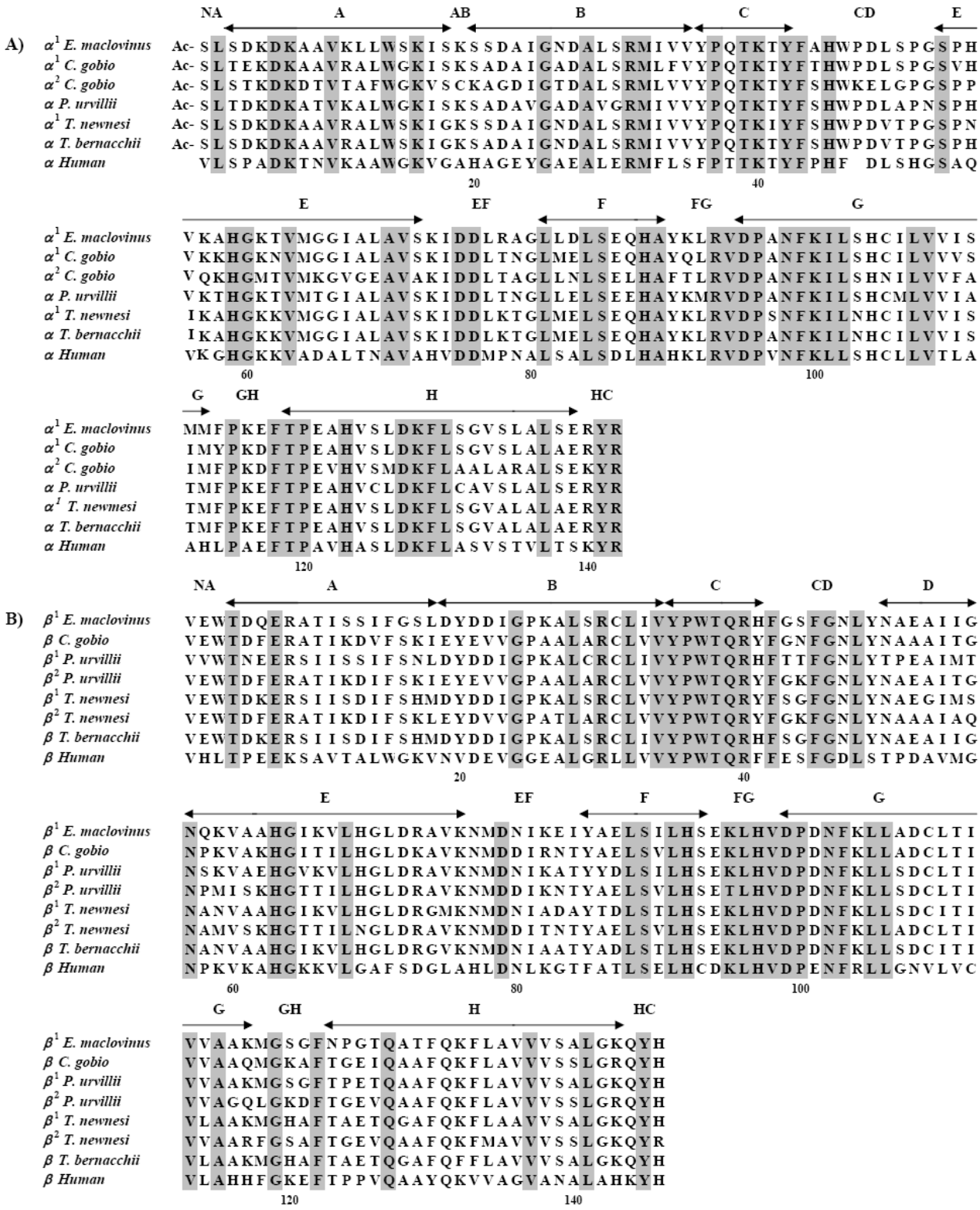

Figure S1. Sequence alignment comparison of *E. maclovinus* α- (A) and β- (B) chains with *C. gobio*, *P. urvillii*, *T. newnesi*, *T. bernacchii* and human HbA α and β chains. Identical residues are in gray.

Kinetics of CO binding and dissociation

Since the behaviour for CO dissociation is closely similar in *Em*Hb1 and *Tb*Hb, for clarity in **Figure S2A** we only report data from *Em*Hb1 and the values from *Tb*Hb are reported in **Table I**.

The behaviour observed in **Figure S3** might be accounted for by the presence of a significant fraction of T-liganded form (likely corresponding to the fast CO dissociating species, **Figure S2A**), progressively destabilised as the temperature rises. Furthermore, CO binding to both *Em*Hb1 and *Tb*Hb does not show any marked subunit heterogeneity, similar to Hbs of Antarctic species belonging to the family Artedidraconidae[5] but in contrast with other temperate-fish Hbs.[6,7] Hence, the observed low affinity for CO binding (**Figure S2B**) is indeed consistent with very high thermodynamic stabilisation of the T-liganded form.

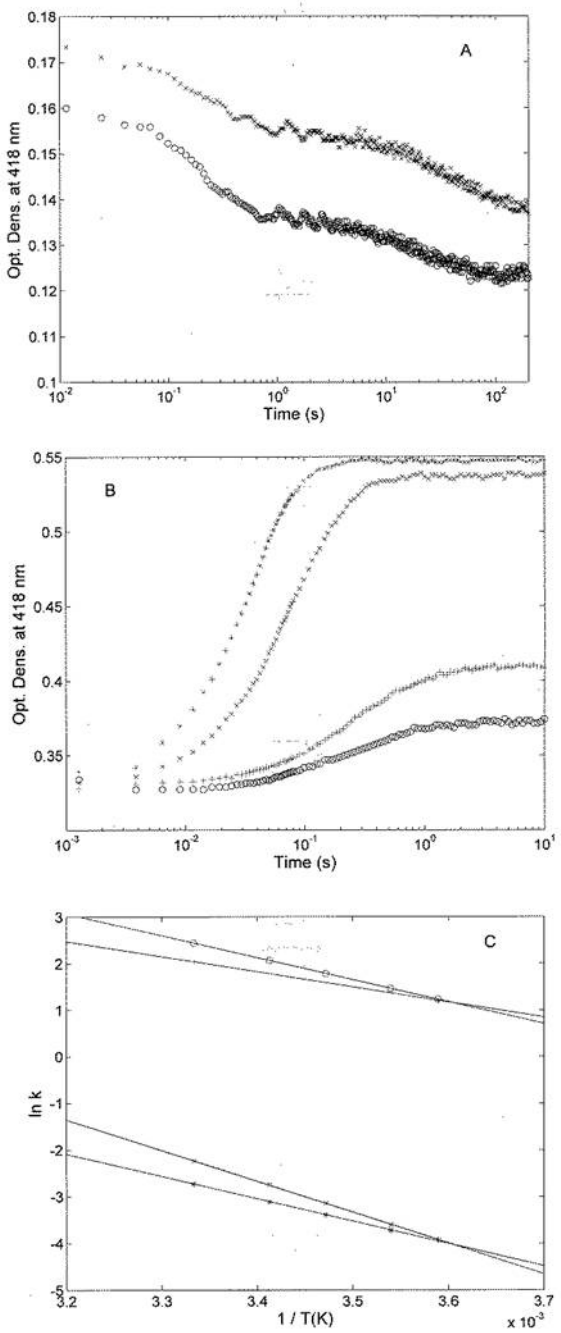

Figure S2 (A) Kinetic progress curves at 418 nm of CO dissociation by NO replacement from *Em*Hb1 in the absence (o) and presence of 3 mM ATP (x), 20°C, in 0.1 M Hepes pH 7.0. Progress curves have been displaced on the *y* axis for clarity. (B) Kinetic progress curves at 418 nm for binding to 5 µM unliganded *Em*Hb1 of different CO concentrations, namely (o) 8 µM, (+) 28 µM, (x) 100 µM and (*) 200 µM. (C) Arrhenius plot of the temperature dependence of the CO-dissociation rate constants by NO displacement from fully liganded *Em*Hb1 in the absence (fast-dissociating species (o) and slow-dissociating species (x)) and presence (fast dissociating-species (+) and slow-dissociating species (*)) of 3 mM ATP, in 0.1 M Hepes pH 7.0. Continuous lines: non-linear least-squares fitting of data according to Eq. (4).

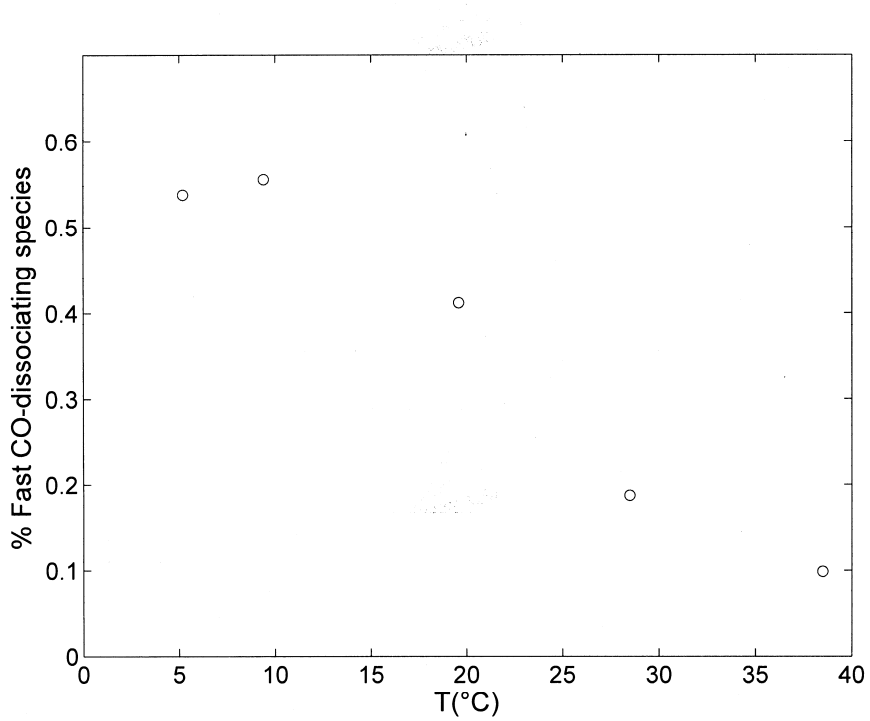

Figure S3. Temperature dependence of the fraction of the faster CO-dissociating species in *Em*Hb1 at pH 7.0.

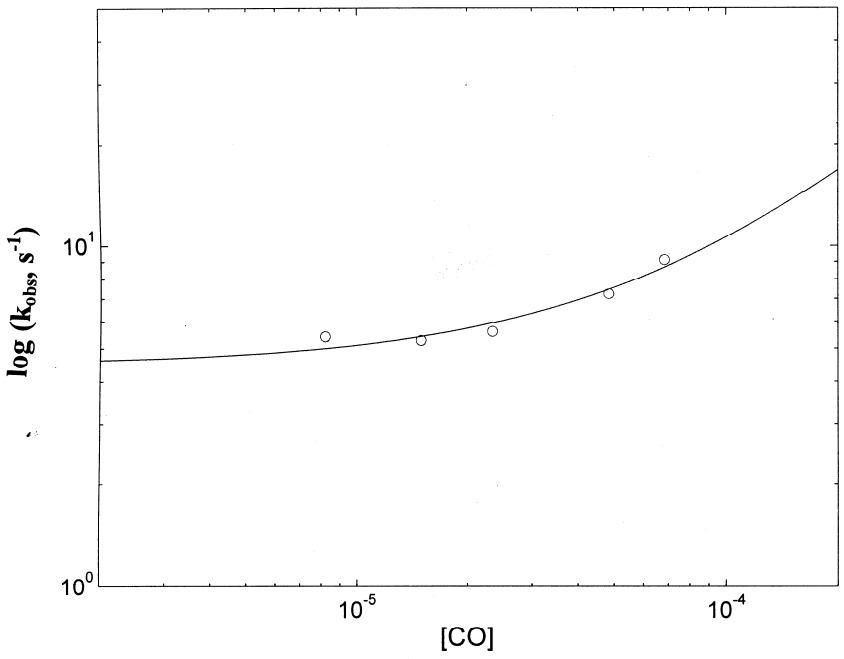

Figure S4. CO-concentration dependence of CO binding to *Em*Hb1 at pH 7.0 and 10°C. The continuous line is the non-linear least-squares fitting of data according to Eq. Y, with k_{on} 6.1(±0.8)×10^4 $M^{-1}s^{-1}$ and k_{off} 4.5±0.6 s^{-1}.

CO-rebinding kinetics

The effect of pH on the amplitudes retrieved from the SVD analysis of the time-resolved spectra collected for *Tb*Hb is shown in **Figure S6**. Above neutral pH, the rebinding kinetics are much faster, while lowering pH to 6.0 results in minor changes. ATP has the largest effect on the rebinding kinetics at pH 8.0. As in *Em*Hb1, second-order rebinding can be described by a linear combination of two exponential decays. The lifetimes are independent of ATP, whereas the amplitude of the slow component increases upon addition of ATP and upon lowering CO concentration. The opposite effect is observed for the amplitude of the fast rebinding species. This is a strong indication that the two rebinding species are the high-affinity R state and the low-affinity T state, respectively. The first-order portion appears unaffected by ATP and was fitted using the sum of two stretched exponential relaxations.

We thus performed a global analysis on the curves retrieved form the experiments in the presence and absence of ATP, holding lifetimes as shared parameters. **Figure S7** shows an example of the fit on the data at pH 8.0. Fitted parameters are reported in **Table SIII**. The data in **Table SIII** allow an estimation to be made of the on-rates to the R- and T-states of *Tb*Hb: $k_{ON,R}$ 2.1×10^5 $M^{-1}s^{-1}$ and $k_{ON,T}$ 0.26×10^5 $M^{-1}s^{-1}$.

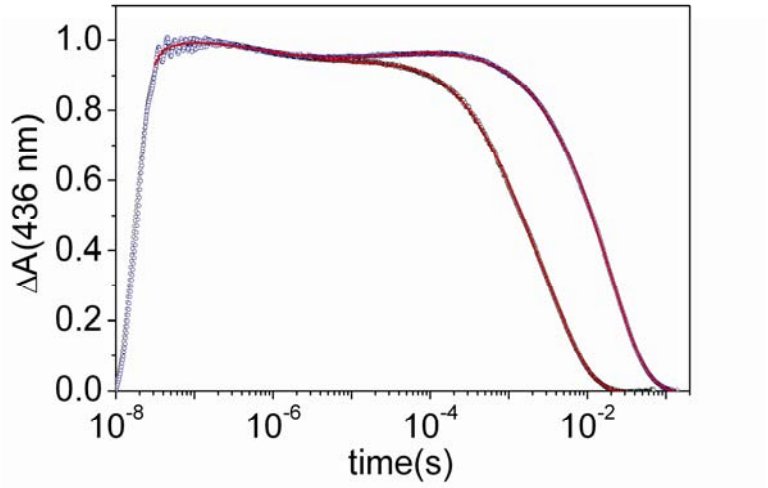

Figure S5. Transient absorbance after nanosecond photolysis of *Em*Hb1-CO solutions equilibrated with 1-atm CO (black) and 0.1-atm CO (blue). Red curves are the result of a fit with a sum of three stretched exponential and two exponential relaxations. T 10°C, pH 7.0.

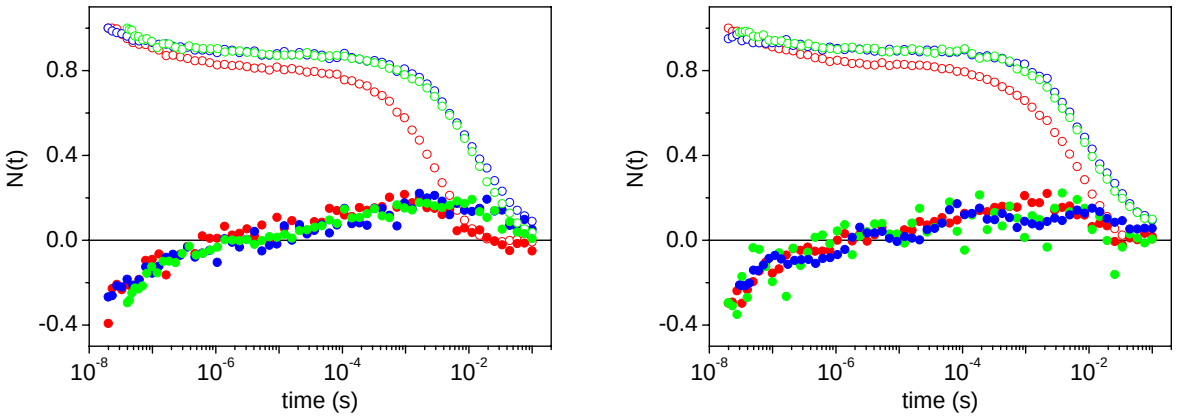

Figure S6. Left panel. Comparison of the time courses of the amplitudes (open circles, component V_1; filled circles, component V_2) determined from the SVD analysis on time-resolved difference spectra collected after photolysis of *Tb*Hb in solution. Green, pH 6.0; blue, pH 7.0; red, pH 8.0. 10 °C, CO 1 atm. **Right panel.** Same, but with 3 mM ATP.

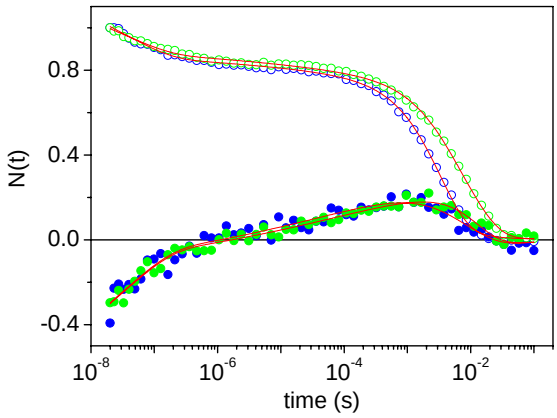

Figure S7 Analysis of the amplitudes (open circles, component V_1; filled circles, component V_2) determined from SVD analysis of time-resolved differential absorption spectra of *Tb*Hb equilibrated with 1 atm CO in the absence (blue) and presence (green) of 3 mM ATP, 10°C, pH 8.0, 1 atm CO. Red curves are the best fit obtained after global analysis of the set of four traces with a four-exponential relaxation with shared lifetimes and stretching exponents.

Table SIII

Lifetimes and relative amplitudes of bimolecular rebinding to R and T for *Tb*Hb, from the global analysis of V_1 and V_2 components at pH 6.0, 7.0, and 8.0, with and without 3 mM ATP. 10 °C; CO 1 atm.

			R (%)	**τ_3 (ms)**	**T (%)**	**τ_4 (ms)**
pH 6.0	**V_1**		33	4.6±0.3	67	37±2
		+ATP	38		62	
pH 7.0	**V_1**		41		59	
		+ATP	44		56	
pH 8.0	**V_1**		100		0	
		+ATP	74		26	

Table SIV.

Full results of the global analysis of the CO rebinding kinetics to *Em*Hb with the equation* $A = A_1 e^{-\left(\frac{t}{\tau_1}\right)^{\beta_1}} + A_2 e^{-\left(\frac{t}{\tau_2}\right)^{\beta_2}} + A_3 e^{-\left(\frac{t}{\tau_3}\right)} + A_4 e^{-\left(\frac{t}{\tau_4}\right)}$ on the set of 12 curves (V_1 and V_2) obtained from the SVD analysis at the three investigated pH values at 10°C and 1 atm CO. Shared parameters were lifetimes and stretching exponents.

			A_1	**τ_1(ns)**	**β_1**	**A_2**	**τ_2 (μs)**	**β_2**	**A_3**	**τ_3 (ms)**	**A_4**	**τ_4 (ms)**
pH 6	V_1		0.07±0.03	49±8	0.7	0.12±0.03	11±9	0.2	0.15±0.02	1.5±0.1	0.70±0.02	16.2±0.1
		+ATP	0.05±0.03			0.08±0.03			0.12±0.02		0.78±0.02	
	V_2		-0.18±0.03			-0.31±0.03			-0.16 ±0.02		0.29±0.02	
		+ATP	-0.18±0.03			-0.17±0.03			-0.22±0.03		0.28±0.01	
pH 7	V_1		0.04±0.03			0.18±0.03			0.76±0.02		0.06±0.01	
		+ATP	0.07±0.03			0.06±0.03			0.41±0.02		0.48±0.01	
	V_2		-0.29±0.03			-0.30±0.03			0.13±0.02		0.04±0.01	
		+ATP	-0.08±0.03			-0.48±0.03			0.03±0.03		0.19±0.02	
pH 8	V_1		0.0003±0.0001			0.32±0.02			0.72±0.02			
		+ATP	0.05±0.03			0.19±0.04			0.30±0.03		0.49±0.02	
	V_2		-0.23±0.04			-0.45±0.03			0.18±0.02		0.05±0.02	
		+ATP	-0.16±0.03			-0.39±0.04			-0.06±0.03		0.25±0.02	

*Following the assumption that the allosteric effector causes a change in the populations of the species formed upon photolysis, but not in their CO-rebinding rates, we have analysed the kinetics with a global approach using a sum of two stretched exponentials and two exponential relaxations. The two relaxations, described by stretched exponential relaxations, occur on nanosecond and microsecond time scales. These are most likely associated with tertiary (ns) and quaternary (μs) relaxations.

Deoxy form and Fe^{2+}-CO complex

To gain insight into the structure of the proximal side of the haem cavity, *Em*Hb1 was studied in the ferrous state at pH 7.6. After reduction, the UV-vis spectrum (**Figure 5A**) is similar to the deoxy species of *Pu*Hb1 (Fe^{2+})[8] and human HbA[9,10] and is characteristic of a 5cHS haem state. Accordingly, the corresponding high-frequency RR spectrum is characteristic of a 5cHS species with bands at 1471 [ν_3], 1524 [ν_{38}], 1564 [ν_2] and 1604 cm^{-1} [ν_{10}] (**Figure S8**).

The low-frequency RR spectrum is shown in **Figure 5B**. The main interest in this region of 5-coordinate haemoproteins is the presence of a strong band due to the iron bound imidazole stretching mode, ν(Fe-Im), in the range 200-250 cm^{-1}. The ν(Fe-Im) stretching mode frequency is very sensitive to hydrogen bonding and, therefore, to the protein matrix surrounding the proximal His.[11,12] In human HbA, the histidyl bond is strained by helix F due to T-state quaternary interactions, as shown by low ν(Fe-Im) frequency at 215 cm^{-1} (**Table SV**).[11] Similarly, the RR low-frequency region of *Em*Hb1 (Fe^{2+}) (**Figure 5B**) is characterised by a strong band at 213 cm^{-1}, not present in the ferric form, assigned to the ν(Fe-Im) iron-histidyl stretching mode. The absence of significant differences in the ν(Fe-Im) stretching frequencies (**Table SV**) between deoxy human HbA, *Em*Hb1 (Fe^{2+}) and *Pu*Hb1 (Fe^{2+})[8] suggests that the proximal cavity in *Em*Hb1 is largely unchanged compared to human HbA and *Pu*Hb1.

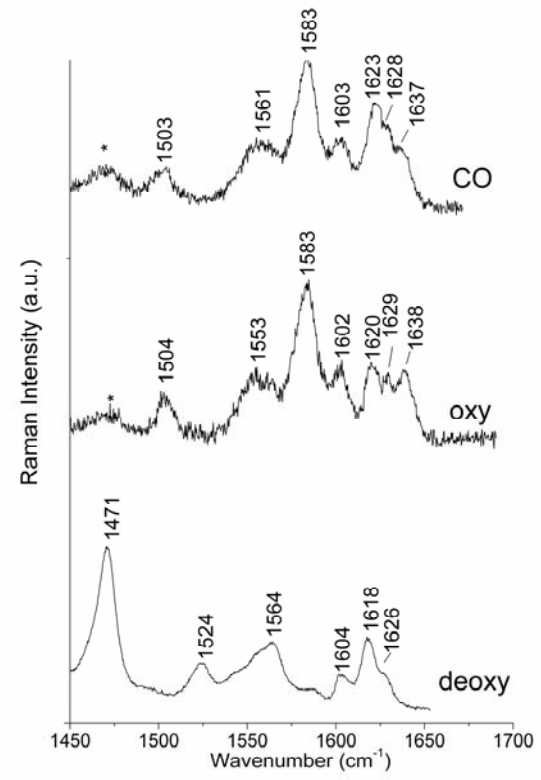

Figure S8. High-frequency region RR spectra of *Em*Hb1 deoxy, (Fe^{2+})-oxy and -CO adducts in 50 mM Tris-HCl pH 7.6. The spectra have been shifted along the ordinate axis to allow better visualisation. Experimental conditions: λ_{exc}: 413.1 nm, 1.2 cm^{-1} spectral resolution. Hb1 (Fe^{2+}) deoxy: 13 mW laser power at the sample, average of three spectra with 480-s integration time. *Em*Hb1 (Fe^{2+})-oxy: 10 mW laser power at the sample (using a cylindrical lens to focus the laser beam), average of eight spectra with 120-s integration time. Hb1 (Fe^{2+})-CO: 3 mW laser power at the sample (using a cylindrical lens), average of two spectra with 300-s integration time. The intensities are normalised to that of the ν_4 band (not shown). The asterisk indicates the spurious band due to the photolysed form.

Table SV.

Comparison of Fe-ligand stretching mode RR frequencies (cm^{-1}) of *Em*Hb1, *Pu*Hb1, human HbA and *Tb*Hb

	***Em*Hb1**[a]	***Pu*Hb1**[8]	**HbA**	***Tb*Hb**
ν(Fe-Im)	213	215	215[11]	N.D.
ν(Fe-O_2)	572	568	568[13]	N.D.
ν(Fe-CO)	502	502	507[14]	502[15]
ν(CO)	1954	1952	1951[14]	1951[b]

[a]This work. [b]Vergara et al., unpublished data.

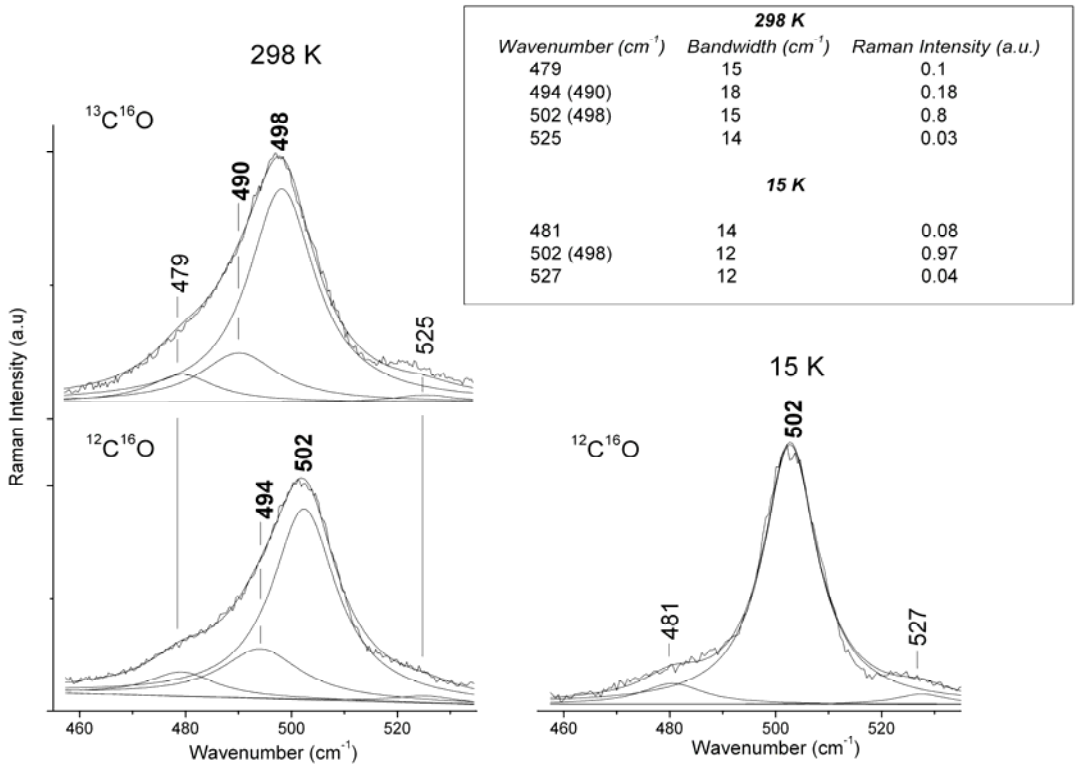

Figure S9. RR spectra in the 460-535 cm^{-1} region and corresponding band-fitting analysis of the ^{12}CO (298 K and 15 K) and ^{13}CO (298 K) complexes of *Em*Hb1 (Fe^{2+})-CO. The spectra have been shifted along the ordinate axis to allow better visualisation. Experimental conditions: for 298 K, see **Figure 5**; for 15 K: λ_{exc} 413.1 nm, spectral resolution 5 cm^{-1}, power at the sample 2 mW, collection interval 8 s/0.5 cm^{-1}. The ν(Fe-C) bands are indicated in bold. In the Table are reported the band fitting parameters. The ^{13}CO ν(Fe-C) frequency is shown in brackets. The bands at 479-481 cm^{-1} were assigned to the ν_{33} B_{2g} mode, the band at 525-527 cm^{-1} to the ν_{25} A_{2g} mode.

A good curve fitting can be achieved either by excessively increasing the bandwidth of the 479 cm^{-1} mode or, more reasonably, introducing a new band at 494 cm^{-1} that shifts to 490 cm^{-1} in the ^{13}CO adduct. The presence of a γ_{12} mode at 492 cm^{-1} can be ruled out since it does not properly fit the spectra of both the ^{12}CO and ^{13}CO adducts. The corresponding ν(CO) stretching mode is tentatively placed at 1970 cm^{-1} (1925 cm^{-1} in ^{13}CO, inset **Figure 5B**) in agreement with IR measurements (data not shown).

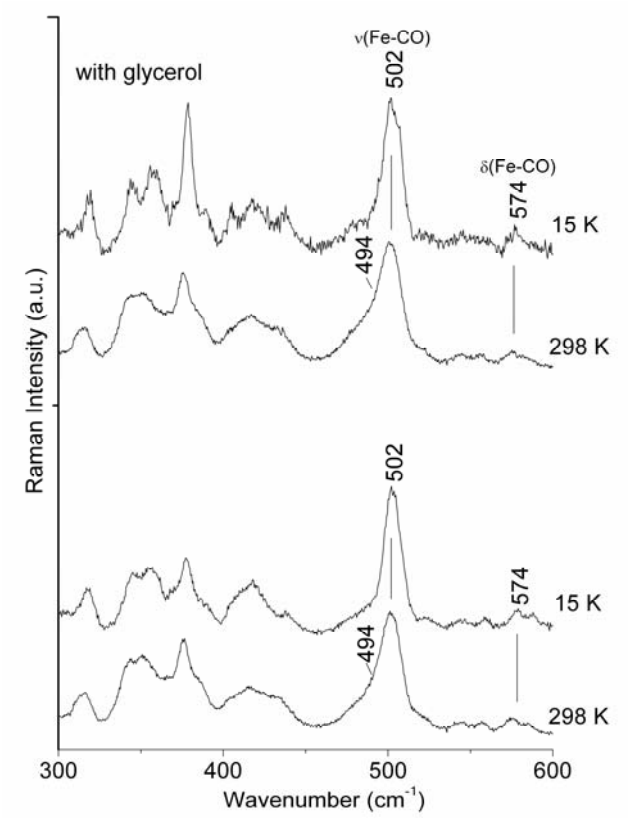

Figure S10. Low-frequency region RR spectra of *Em*Hb1 (Fe^{2+})-CO adducts in 50 mM Tris-HCl pH 7.6, in the absence and presence of 22% (v/v) glycerol, at 298 and 15 K. The spectra have been shifted along the ordinate axis to allow better visualisation. Experimental conditions: for samples without glycerol see **Figures 5 and S9**. For samples with glycerol: λ_{exc}: 413.1 nm, 1.2 cm^{-1} spectral resolution, 3 mW laser power at the sample (using a cylindrical lens), average of three spectra with 700-s integration time (298 K); 5 cm^{-1} spectral resolution, 0.8 mW laser power at the sample, collection interval 20 s/0.5 cm^{-1} (15 K).

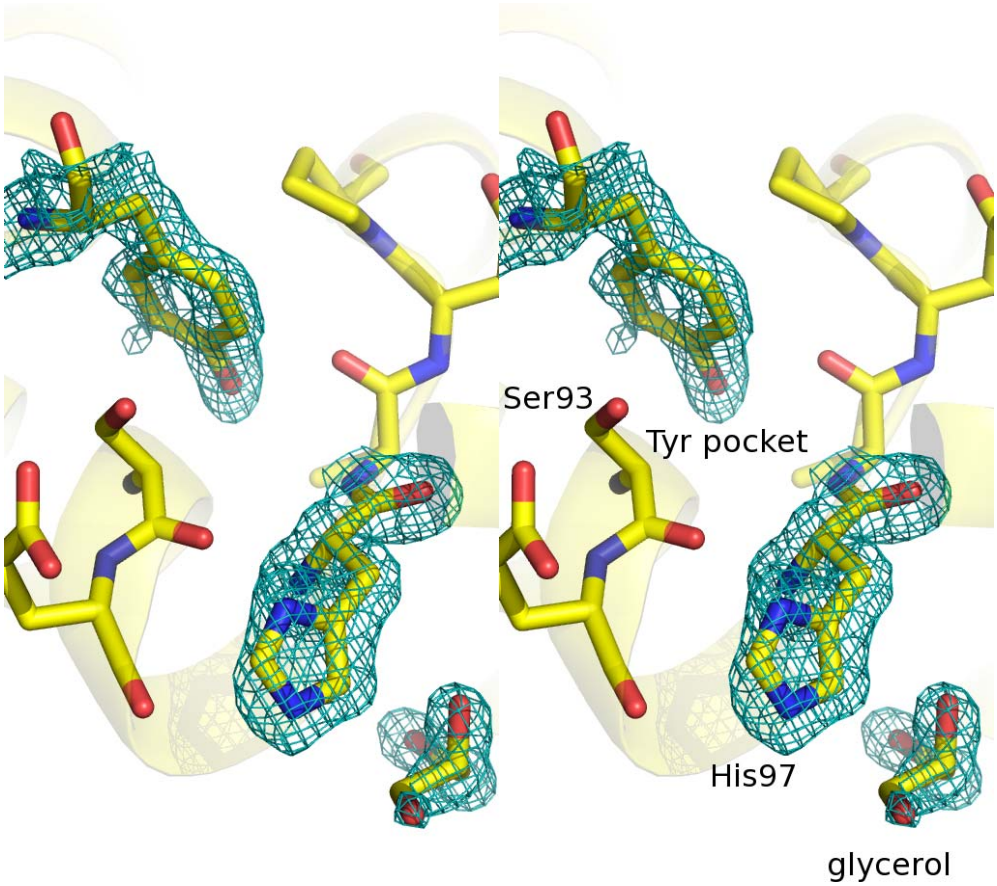

Figure S11. 2Fo-Fc electron-density maps (1σ) showing the position of glycerol and of the tyrosyl pocket.

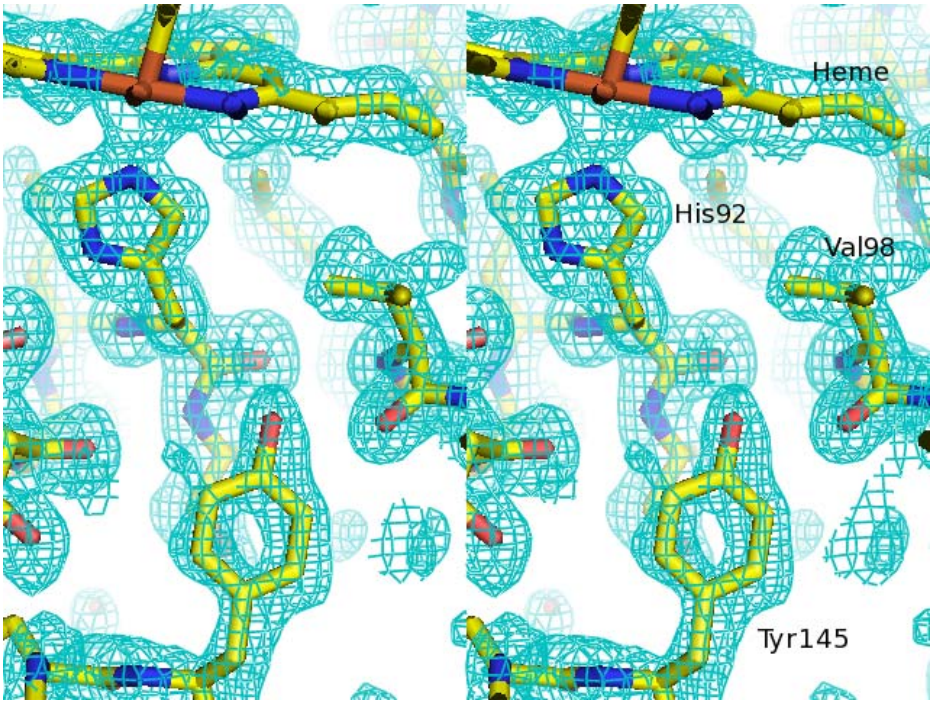

Figure S12. 2Fo-Fc electron-density map (1.2σ) of the tyrosyl pocket of the β_2 chain

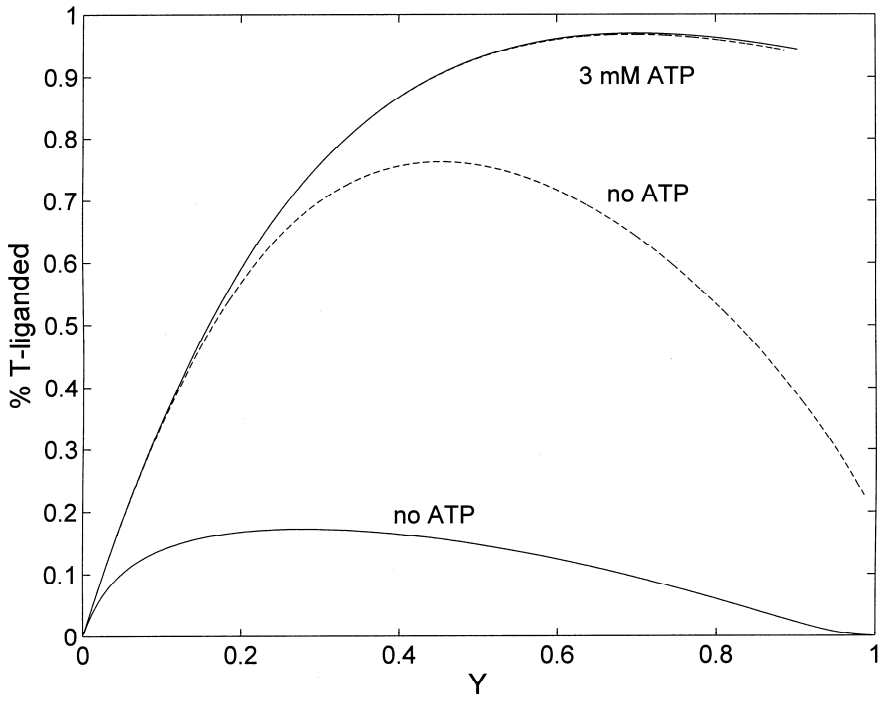

Figure S13. Percentage of T-liganded forms as a function of O_2 saturation degree (Y) for *Em*Hb1 (continuous lines) and *Tb*Hb (dashed lines) according to thermodynamic parameters reported in the legend of **Figure 2** in the absence and presence of 3 mM ATP, as indicated.

References

1 J. Navaza, *Acta Cryst.*, 1994, **A50**, 157-163.
2 A. Merlino, L. Vitagliano, B. D. Howes, C. Verde, G. di Prisco, G. Smulevich, F. Sica and A. Vergara, *Biopolymers*, 2009, **91**, 1117-1125.
3 G. Sheldrick and T. Schneider, *Meth. Enz.*, 1997, **277**, 319-343.
4 T. A. Jones, J. Y. Zou, S. W. Cowanand and M. Kjedgaard, *Acta Cryst. D: Biol. Cryst.*, 1991, **56**, 714-721.
5 M. Tamburrini, M. Romano, V. Carratore, A. Kunzmann, M. Coletta and G. di Prisco, *J. Biol. Chem.*, 1998, **273**, 32452-32459.
6 B. Giardina, G. M. Giacometti, M. Coletta, M. Brunori, G. Giacometti and G. Rigatti, *Biochem. J.*, 1978, **175**, 407-412.
7 M. Coletta, P. Ascenzi, R. D'Avino and G. di Prisco, *J. Biol. Chem.*, 1996, **271**, 29859-29864.
8 C. Verde, B. D. Howes, M. C. De Rosa, L. Raiola, G. Smulevich, R. Williams, B. Giardina, E. Parisi and di G. Prisco, *Prot. Sci.*, 2004, **13**, 2766-2781.
9 M. F. Perutz, J. E. Ladner, S. R. Simon and C. Ho, *Biochemistry*, 1974, **13**, 2163-2173.
10 T. G. Spiro and T. C. Strekas, *J. Am. Chem. Soc.*, 1974, **96**, 338-345.
11 T. Kitagawa, in *Biological Applications of Raman Spectroscopy: Resonance Raman Spectra of Haems and Metalloproteins*, ed. T. G. Spiro, Wiley, New York,1988, pp. 97-131.
12 G. Smulevich, J. M. Mauro, L. A. Fishel, A. M. English, J. Kraut and T. G. Spiro, *Biochemistry*, 1988, **27**, 5477-5485.
13 C. H. Robert, L. Fall and S. J. Gill, *Biochemistry*, 1988, **27**, 6835-6843.

14 E. Antonini and M. Brunori, in *Haemoglobin and myoglobin and their reactions with ligands*, eds. A. Neuberger and E. L. Tatum, North Holland, Amsterdam, 1971, pp. 17-19.
15 A. Merlino, L. Vitagliano, B. D. Howes, C. Verde, G. di Prisco, G. Smulevich, F. Sica and A. Vergara, *Biopolymers*, 2009, **91**, 1117-1125.